Reconstruction of 3D Brain Structures from Clinical 2D MRI Data

Rui Shi[1] [a], Tsukasa Koike[2] [b], Tetsuro Sekine[3] [c], Akio Morita[4] [d] and Tetsuya Sakai[1] [e]

[1]*Department of Computer Science and Engineering, Waseda University, Shinjuku, Tokyo, Japan*
[2]*Department of Neurosurgery, Teraoka Memorial Hospital, Fukuyama, Hiroshima, Japan*
[3]*Department of Radiology, Nippon Medical School Musashi Kosugi Hospital, Kawasaki, Kanagawa, Japan*
[4]*Tokyo Rosai Hospital, Ota, Tokyo, Japan*

Keywords: Brain MRI, 3D Reconstruction.

Abstract: As the population is aging worldwide, the number of dementia patients increases. Brain MRI is expected to play a crucial role in the prediction of dementia at an early stage. Current 3D brain structure reconstruction methods have strict rules and require a large number of slice images. Routine clinical MRI files contain much fewer slices, but diagnosis relies heavily on information obtained from MRI scans. In this paper, we proposed a method that is able to reconstruct the 3D brain structure with 2D DICOM MRI images within the clinical routine budget, by applying trilinear interpolation. The generated images and structures are evaluated with PSNR and SSIM. The results show that although the details in the generated 2D slices are not ideal, our method is able to reconstruct 3D structures that are highly similar to the original brain structures using only one-fifth of the image slices.

1 INTRODUCTION

Population around the world is aging. For example, in Japan, the proportion of people aged 65 and over exceeds one-quarter of the total population (Statistics Bureau, 2023). Providing proper medical care for senior citizens is a major issue and needs to be addressed with contributions from society.

Dementia is one of the most common mental illnesses that afflict the elderly, which causes a decline in cognitive abilities and has negative impacts on the individual in various ways, such as mobility, emotion, and social relationships (van der Flier and Scheltens, 2005). Since dementia is slowly progressive (Bathini et al., 2019), if diagnosed at the early stage, the development of the disease can be eased with intervention. Such prediction models are expected to be developed with Brain MRI images.

Magnetic resonance imaging (MRI) technology has been used for decades to obtain high-quality brain images. Compared to other diagnostic imaging techniques, MRI does not expose patients to radiation in Positron Emission Tomography (PET) (Carlson

and Carlson, 2007), and provides better tissue contrast than Computed Tomography (CT) Scanner (Ebel and Benz-Bohm, 1999). Various information can be obtained through Brain MRI, such as the changes in white matter which reflect systemic hypertension (Salerno et al., 1992).

MRI scans divide the brain into slices at given intervals, where each slice shows a 2D scan image of the corresponding location. During the slicing process, 3D characteristics of the patient's brain can be lost. The volume and proportions become difficult to quantify, and the spatial relationships between different parts are unclear. But most current diagnoses and surgery plans are based on MRI scans. Hence, it is essential to reconstruct the 3D structure of the brain for accurate presentation and alignment.

DICOM is the standard format used in hospitals and clinics for MRI (Mustra et al., 2008). If the 3D brain structure is reconstructed by simply stacking the slice images according to their location, at least 100 slices are required for each coordinate axis, or a total of more than 300. However, in clinical routine, DICOM MRI files are usually generated with only 19 slices along one single coordinate axis for financial and waiting time considerations. Diagnoses based on such files highly depend on the expertise and experience of the doctor.

To fill the gap and better assist doctors in diagnosis and surgery decisions, in this work, we propose a

[a] https://orcid.org/0009-0002-7339-0305
[b] https://orcid.org/0000-0002-9931-0716
[c] https://orcid.org/0000-0003-1547-6696
[d] https://orcid.org/0000-0002-2497-5772
[e] https://orcid.org/0000-0002-6720-963X

method to reconstruct the 3D brain structure with 2D MRI images at a relatively low cost, with a limited number of slices within the clinical routine budget, while aiming for high quality, accuracy, and speed.

2 PRELIMINARIES

2.1 Background

2.1.1 Metadata in DICOM Files

Each DICOM file has a metadata header, providing information such as slice spacing and dimension. To achieve success in 3D reconstruction by stacking the 2D slices, the required number of slices exceeds what is obtained in most routine clinical MRI DICOM files, and the metadata of the slices must match in a highly accurate order (AlZu'bi et al., 2020). However, vibration during the scan process and variations between acquisition devices can lead to divergences and inaccuracies in the metadata.

In addition, routine clinical MRI slices are mostly separated with relatively large spacing, leaving the structures between the intervals vacant. By simply stacking the images, the generated structure is discontinuous because of the information lost in the intervals, and differs largely from the actual structure.

2.1.2 Bias Field and Noise

Bias field exists during MRI scans, especially those taken by old MRI machines. Such uneven intensity produces smooth, low-frequency signals that interfere with the MRI scanning process (Juntu et al., 2005). Bias field can cause intensity variation among homogeneous tissues, which changes high-frequency components such as contours and edges, causing blurs in the images. The variation may not be easily observed but can result in the decline of feature points during image processing.

Also, the RF emission from the thermal motion of the patient's body causes much inevitable noise in the scanned MRI images, which appears as irregular granular patterns and confuses information acquisition (Aja-Fernández and Vegas-Sánchez-Ferrero, 2016).

2.2 Related Work

2.2.1 Pre-Processing of Image

Histogram equalization is often used to counteract the effects of bias fields (Senthilkumaran and Thimmiaraja, 2014). It is a general method used for grayscale image enhancement, performed with the cumulative distribution function (CDF) of intensity. Since image voxels in DICOM files are encoded by intensity, they resemble the grayscale images, which share the same color channel. The images processed by histogram equalization will have higher contrast than the original images.

Noise filters are also widely used to improve the quality of scanned images. There are various types of noise filters, realized with different approaches. For example, in the work of Thanh and Hai (Thanh and Hai, 2017), a mean-unsharp filter, which is convoluted with the 2D MRI images, is applied to remove the noise.

2.2.2 Marching Cube

Marching cubes is a classic computer graphics algorithm that can produce high-resolution 3D surfaces with simple construction operations (Lorensen and Cline, 1998). Even in recent years, this algorithm has shown good performance in reconstructing 3D knee surfaces and spine structures from 2D CT images (Patel and Mehta, 2012), but the calculation will be slow if a large amount of 2D data is processed.

2.2.3 Interpolation

Interpolation is a mathematical approach to estimate unknown points based on the existing points. By constructing a continuous function that passes through the given data points, unknown points between the given data points can be approximated with a high accuracy (Davis, 1975). In Ghoshal's work (Ghoshal et al., 2020), highly accurate 3D reconstruction of spine is achieved by combining the Marching cubes algorithm and interpolation. Although not quantified, reconstruction works of 3D brain structure from 2D MRI images have also received satisfying results using trilinear interpolation (Fajar et al., 2022) (Thanh and Hai, 2017).

3 METHOD

In this section, we propose a method that is able to reconstruct the 3D brain structure from a small amount of 2D DICOM MRI images along one single coordinate axis. Figure 1 shows the four steps taken to accomplish the process, which are introduced in detail.

3.1 Pre-Processing of Image

We propose two alternative approaches for contrast enhancement and noise cancellation. Approach A in-
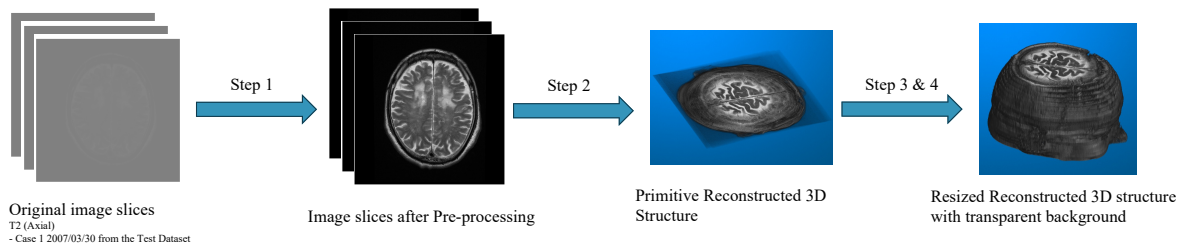
Figure 1: Workflow of 3D Brain Reconstruction from Clinical 2D MRI Image data. 1) Pre-processing of the image; 2) Reconstruction of 3D structure with Trilinear Interpolation; 3) Resizing the generated 3D Image; 4) Making the Background Transparent. The demonstrated original images are from the MRI record collected on *Patient Case 1* from the Test Dataset on March 30, 2007. Further information on the Test Dataset can be found in Section 4.

volves histogram equalization and a noise filter, while Approach B comprises only one contrast filter.

3.1.1 Histogram Equalization

Histogram equalization is applied to enhance the contrast in the images. Considering in a discrete grayscale image x, the probability of the occurrence of a pixel of level i in the image is:

$$p_x(i) = p(x = i) = \frac{n_i}{n}, 0 \leq i < L \qquad (1)$$

where L is the maximum pixel value, n_i is the number of occurrences of the pixel of level i, and n is the number of pixels in the image.

As an MRI DICOM image is similar to a grayscale image with intensity ranging from 0 to 255 for every voxel, L equals the intensity level bound 256. The CDF for the intensity v can be calculated as

$$\text{cdf}_x(v) = \sum_{j=0}^{v} p_x(x = j) \qquad (2)$$

The histogram-equalized intensity value $h(v)$ is derived as

$$h(v) = \text{round}(\text{cdf}_x(v) \cdot (L - 1)) \qquad (3)$$

Through histogram equalization, the equalized intensity value replaces the original value, distributing the pixels more evenly throughout the full range, which gives the image a higher contrast.

3.1.2 Noise Filter

Our noise filter is developed with homogenization of the background.

First, we verify the boundary of the skull. As the objects within the head are separated from the background by the skull, which preserves a much brighter shade than the surrounding background, we can easily measure the intensity value of the skull and set the value as a threshold.

Once the threshold is obtained, the head boundary can be detected. The noise or irrelevant background can be effectively removed by setting all pixels outside the identified boundaries to zero.

3.1.3 Contrast Filter

An alternative way to enhance the contrast and cancel the noise in one step is to use a contrast filter. We designed a contrast filter that adjusts the image contrast by normalizing the pixel values to the full 8-bit range 0 to 255.

First, we find the maximum and minimum pixel values in the image, and calculate the range of variance in pixel value by subtracting the minimum value from the maximum value.

Then, we subtract the minimum pixel value from each pixel and divide the subtraction results by the range of pixel value variance to normalize the pixel values to 0 to 1.

Finally, we multiply the division results by 255 to scale the normalized values into 0 to 255.

Through the contrast filter, the pixels are distributed more evenly to the full range, and the abrupt variance caused by noise is also mostly reduced, canceling noise during the normalization process.

3.2 Reconstruction of 3D Structure with Trilinear Interpolation

After pre-processing, the 2D image slices are now ready to be primitively combined to form the 3D structure.

First, the 2D image slices are stacked according to their slice location shown in the metadata. When image data are simply stacked, there is much empty space with missing information at the intervals between the slices. As the intervals are large for routine clinical MRI images, the spacing may vary between slices.

These empty intervals can be filled with the slices generated by trilinear interpolation, which reconstructs the 3D information between the slices and smoothens the structure. The aim is to approximate
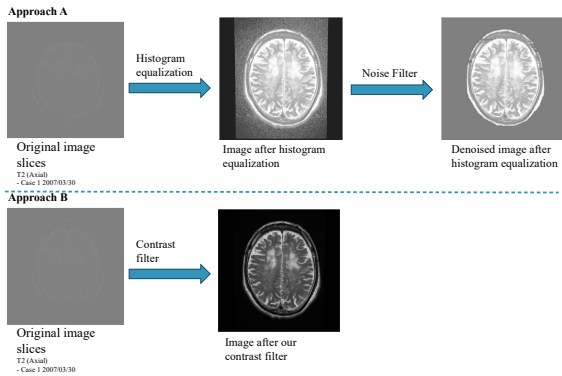
Figure 2: Workflows of the Alternative Approaches (Approach A and Approach B) for Contrast Enhancement and Noise Cancellation. Approach A first applies Histogram Equalization to the original image, then passes the equalized image through the Noise Filter. Approach B only passes the original image through the Contrast Filter. The demonstrated original image is one slice from the MRI record collected on *Patient Case 1* from the Test Dataset on March 30, 2007.

the original 3D structures with our interpolated structures.

Trilinear interpolation is a method of multivariate interpolation on a 3D regular grid (Davis, 1975). It can predict the pixel value of any point within the 3D structure with a faster speed than the Marching cube (Rajon and Bolch, 2003), as follows:

Considering in a unit-size cubic lattice, a point located at (u,v,w) in the spatial domain expects pixel prediction by trilinear interpolation, as shown in 3.
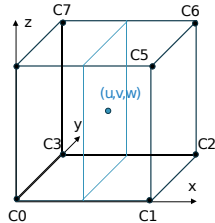

Figure 3: An example of Trilinear Interpolation within a unit-size cubic lattice. The 3D Cartesian coordinate system is formed by the x, y, and z axes. The C_n values are the pixel values of the vertices, where n is the index for each vertex. The point located at (u,v,w) is expecting pixel prediction.

The pixel value $C(u,v,w)$ of the point located at (u,v,w) is calculated as:

$$
\begin{aligned}
C(u,&v,w) \\
=&C_0(1-u)(1-v)(1-w)+C_1u(1-v)(1-w) \\
&+C_2uv(1-w)+C_3(1-u)v(1-w) \\
&+C_4(1-u)(1-v)w+C_5u(1-v)w \\
&+C_6uvw+C_7(1-u)vw
\end{aligned} \tag{4}
$$

3.3 Resizing 3D Image

The default setting makes the primitive reconstructed 3D structure a plate. Therefore, resizing is needed to adjust the structure to the proper scale. We adjust the proportions of the head referencing biostatistics data (Bail et al., 2009) and uniformize the size and resolution of the generated 3D brain structures.

3.4 Making the Background Transparent

During the pre-processing step, we evenly enhanced the image contrast, where the pixels representing the objects within the head preserved a much different intensity level from the pixels representing the background. We can set the pixels within the background level to 0 to make the background transparent easily and efficiently, so that the brain structure can be clearly viewed from all angles and is emphasized.

4 EXPERIMENT

In this section, the details of our experiments are clarified.

4.1 Dataset

In this research, we use a Test Dataset and an Evaluation Dataset. Both datasets are collected from the Teraoka Memorial Hospital in Hiroshima, Japan.

4.1.1 Test Dataset

The Test Dataset consists of 115 records of 2D MRI DICOM files. Nineteen volunteers have contributed to this dataset through the years.

Each 2D MRI DICOM file in this dataset includes 19 slices at a spacing interval of 5 mm. There are three types of data scanned along the coordinate axes: (1) The Axial data is collected along the vertical axis, from the top to the bottom of the head; (2) The Coronal data is collected along one horizontal axis, from the back to the front of the head; (3) The Sagittal data is collected along the other horizontal axis, orthogonal to the Coronal axis, from the side of the head.

This dataset is used to verify whether our method is adaptable to all kinds of data, as there is a relatively rich number of samples and a variety of data types in this dataset.

4.1.2 Evaluation Dataset

The Evaluation Dataset consists of 22 records of 3D MRI DICOM files for evaluation. This dataset is contributed by twenty-two volunteers.

In this dataset, there are 22 records of 3D Sagittal data. Each record of such data includes approximately 100 slices, spaced with an interval of 1 mm.

This dataset is used to evaluate the generation performance quantitatively. With this dataset, by taking samples from the 3D Sagittal data, we can not only obtain the similarity of the entire structure between the original form and the generated form, but also the similarity between the generated slice and the original slice. In addition, if we take the first slice in every five slices as a sample, we can create a sampled 2D set containing approximately 20 slices, similar to the routine clinical file containing 19 slices. Hence, we can expect similar performance in reconstructing 3D brain structure using the proposed method, with routine clinical MRI data.

4.2 Evaluation Metrics

Two evaluation metrics are applied to validate the results.

4.2.1 Peak Signal to Noise Ratio (PSNR)

Peak signal-to-noise ratio (PSNR) is an image evaluation measure. It is often used to calculate the visual error between two images, such as measuring the visual difference between the original image and the compressed image, the difference between the image generated by the generative network and the actual image, etc.

PSNR is defined via the mean squared error (MSE). Suppose there are two $m \times n$ monochrome images I and K, I is noiseless and K is similar to I but contains noise. MSE between I and K is defined as

$$MSE(I,K) = \frac{1}{mn} \sum_{i=0}^{m-1} \sum_{j=0}^{n-1} [I(i,j) - K(i,j)]^2 \quad (5)$$

where $I(i,j)$ and $K(i,j)$ are the pixel values at position (i,j) (i-th row and j-th column) in I and K respectively.

PSNR is defined in units of dB, as

$$PSNR(I,K) = 10 \cdot \log_{10} \frac{(MAX_I)^2}{MSE} \quad (6)$$

where MAX_I is the maximum pixel value of the original image.

PSNR is always non-negative and equals infinity when the two images are identical (Bull and Zhang, 2014). The higher the PSNR value, the less noise in the noisy image. PSNR is a pixel-wise metric: if the pixel value is different, it will be considered as noise and quantified.

4.2.2 Structural Similarity Index Measure (SSIM)

Structural similarity index measure (SSIM) is another metric for measuring the similarity between two images. SSIM performs the comparison from a structural perspective, considering brightness, contrast, and structural information in the images (Wang et al., 2004). Structural information assumes that pixels have strong inter-dependencies, especially when spatially close.

Suppose there are two images x and y, SSIM between x and y is defined as

$$SSIM(x,y) = [l(x,y)]^\alpha [c(x,y)]^\beta [s(x,y)]^\gamma \quad (7)$$

where
$l(x,y) = \frac{2\mu_x\mu_y + C_1}{(\mu_x)^2 + (\mu_y)^2 + C_1}$ compares the brightness between x and y;
$c(x,y) = \frac{2\sigma_x\sigma_y + C_2}{(\sigma_x)^2 + (\sigma_y)^2 + C_2}$ compares the contrast between x and y;
$s(x,y) = \frac{\sigma_{xy} + C_3}{\sigma_x\sigma_y + C_3}$ compares the structure similarity between x and y;
α, β, γ are the positive parameters for adjustment;
μ_x, μ_y are the pixel sample means of x and y;
σ_x, σ_y are the standard deviations of x and y;
σ_{xy} is the covariance of x and y;
C_1, C_2, C_3 are constants to stabilize the division with a weak denominator.

The higher the SSIM value is, the higher the similarity the two images preserve. The maximum value of SSIM is achieved when the two images are identical, and the SSIM value can be negative when the structural information in the two images differs too much.

5 RESULTS

In Section 2, we proposed two alternative approaches for pre-processing. Figure 4 shows the processed images for a record with Approaches A and B, respectively.

Both the original and the generated 3D brain structure can be presented and observed from all angles after the execution of the implemented program. Figure 5 shows a sample of the original and the generated 3D brain structures from the same record.
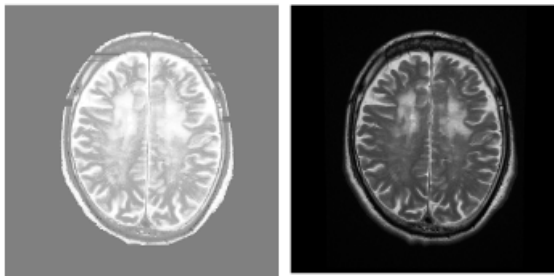
(a) Denoised image after histogram equalization. (b) Image after our contrast filter.

Figure 4: The 2D MRI images pre-processed with alternative approaches for Contrast Enhancement and Noise Cancellation. (a) Approach A, first applying Histogram Equalization to the original image, and then passing the equalized image through the Noise Filter. (b) Approach B, which only passes the original image through the Contrast Filter. The demonstrated images came from the same original image, one slice from the MRI record collected on *Patient Case 1* from the Test Dataset on March 30, 2007.
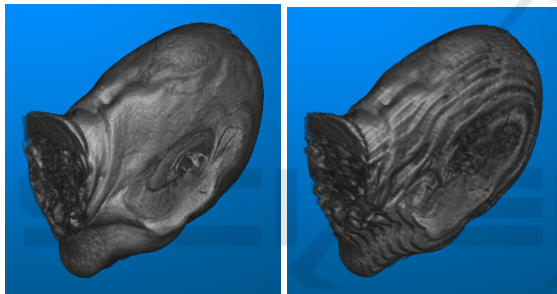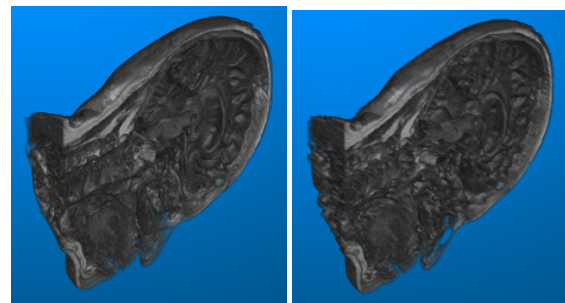

(a) Original structure. (b) Generated structure.

Figure 5: An example of the Original and the Generated 3D Brain Structures from the Same Record. The left diagram shows the original 3D brain structure stacked with 103 slices along the corresponding axis. The right diagram shows the interpolated 3D brain structure generated with 21 sampled slices along the same axis. The image data used by both diagrams came from the same MRI record collected on *Patient Case 01* from the Evaluation Dataset.

Cross-sections can also be cut at arbitrary positions in the original and the generated 3D brain structure, allowing observation from all angles. Figure 6 shows a sample of the original and the generated 2D brain slices from the same record.

Calculation results of the PSNR and SSIM values are printed out after execution of the implemented program. Figure 7 presents an example showing part of the output.

The average PSNR and SSIM results for each patient are summarized in Table 1. The *PSNR* and *SSIM (Structure)* values are obtained by comparing the original and the generated 3D brain structures. The *SSIM (Slices)* values are obtained by comparing slice by slice.

(a) Original structure. (b) Generated structure.

Figure 6: An example of the Original and the Generated 2D Brain Slices from the Same Record. The left diagram shows a cross-section in the original 3D brain structure, while the right diagram shows the cross-section at the same position, from the same angle, in the interpolated 3D brain structure. The image data used by both diagrams came from the same MRI record collected on *Patient Case 01* from the Evaluation Dataset.

```
>> dicom2Dvs3D
PSNR   22.3744, SSIM   0.8900
ID  1, PSNR   Inf, SSIM  1.0000
ID  2, PSNR  24.8231, SSIM  0.3891
ID  3, PSNR  21.2155, SSIM  0.3375
ID  4, PSNR  21.0515, SSIM  0.3473
ID  5, PSNR  23.9589, SSIM  0.3786
ID  6, PSNR   Inf, SSIM  1.0000
ID  7, PSNR  24.0934, SSIM  0.3467
ID  8, PSNR  20.3372, SSIM  0.3008
ID  9, PSNR  19.6618, SSIM  0.2962
ID 10, PSNR  21.9472, SSIM  0.3627
```

Figure 7: An example showing partial output. The values in the yellow-marked area are obtained by comparing the original and the generated 3D brain structures as an overview. The rest of the output with *ID*s are obtained by making the comparison slice by slice, between the original slices and the corresponding slices at the same position from the interpolated 3D brain structure. The values in the blue-marked areas are the results of the sampled slices. These results are excluded from the statistical analysis later on. This output is generated based on the data from the MRI record collected on *Patient Case 01* from the Evaluation Dataset.

6 DISCUSSION

6.1 Approach for Pre-Processing

Qualitatively, the image after our contrast filter preserved distinctively more complete objects and shows higher contrast. On the contrary, the denoised image has a lower contrast after histogram equalization, and the objects have missing parts.

Hence, Approach B, which applies our contrast filter, is chosen and used for the pre-processing.

Table 1: Average PSNR and SSIM results for each patient from the Evaluation Dataset.

Patient No.	PSNR	SSIM (Structure)	SSIM (Slices)
01	22.3744	0.8900	0.5686
02	22.3910	0.8781	0.5633
03	21.3912	0.8632	0.5398
04	21.9015	0.8878	0.5623
06	23.3431	0.8752	0.5476
08	22.0405	0.8249	0.5362
09	22.3152	0.8981	0.5854
010	23.0736	0.8863	0.5773
012	22.6628	0.8423	0.5405
S1	22.8207	0.8808	0.5883
S2	22.5581	0.8906	0.5692
S3	22.2656	0.8381	0.5102
S4	24.0652	0.8618	0.5719
S5	23.0599	0.8792	0.5344
S6	20.7212	0.7676	0.5241
S7	19.3878	0.7326	0.4919
S8	22.5163	0.8869	0.5752
S9	24.1441	0.8653	0.5427
S13	22.7782	0.8797	0.5608
S14	22.4127	0.8727	0.5385
S15	22.3385	0.8202	0.5078
S16	23.3206	0.8918	0.5401
Mean	22.4492	0.8597	0.5489
Variance	1.0060	0.0017	0.0006

6.2 Adaptability, Stability and Computational Speed

The proposed method shows high adaptability, succeeding in 3D brain structure generation based on all three types of data scanned along different coordinate axes in the Test Dataset, with images containing approximately 20 slices.

Performance stability can be perceived from 5b: despite some deviations among the patient cases in *PSNR*, only minor variance appears in *SSIM (Structure)* and *SSIM (Slices)* measurement.

The computation is also efficient. The average time to generate the original 3D structure and the reconstructed structure, and compute the PSNR and SSIM values is within 2 seconds.

6.3 Pixel Similarity

The pixel similarity between the generated and the original 3D structure is reflected by *PSNR*. The average PSNR value among all 22 cases of patients in the Evaluation Dataset equals 22.45. Typical values for the PSNR in lossy image and video compression are between 30 and 50 dB, the higher the PSNR value, the better quality the noisy image has (Faragallah et al., 2020). Since there are fewer reference points in the interpolation-generated images, the PSNR values are generally lower (Jung and Yoo, 2009). Furthermore, the objects inside the brain mainly consist of soft tissues, which can be in small scales and various shapes, yet have complicated spatial relationships (adjacent and overlapping) (Nowinski, 2011). Considering the delicacy of the brain structure, the obtained PSNR result and thus the pixel similarity are acceptable.

6.4 Structural Similarity

The structural similarity between the generated and the original 3D structure is shown by *SSIM (Structure)*. The average SSIM among the patients in the Evaluation Dataset is 85.97%, with a minor variance of 0.2%. This indicates that the generated brain structure can stably achieve 85.97% similarity to the original 3D brain structure consisting of a relatively large number of images (approx. 100), based on only relatively few images (approx. 20, one-fifth of the ground-truth). This achievement can be considered inspiring.

The structural similarity between the generated and the original 2D slices is reflected by *SSIM (Slice)*. The average SSIM among the patients is 54.89%, along with a minor variance of 0.1%. This indicates that the generated image slices can stably achieve 54.89% similarity to the original slices at the same position. Unlike the remarkable resemblance in the overview of the 3D structure, in a 2D slice perspective, the generated images lack much more similarity to the original slices.

One possible explanation for the gap between the 2D and 3D performance could be that, although the sampled data has large spacing intervals between the slices, the slices still manage to cover the information for the entire brain, among which the major characteristics that matter in the 3D structure are still preserved. However, linear prediction cannot precisely regenerate the details on a 2D slice within the empty intervals, with limited information of that localized area being only two adjacent slices.

7 CONCLUSION

We proposed a low-cost method to reconstruct the 3D brain structure with routine clinical 2D MRI images, using trilinear interpolation. The results indicate that our method delivers good performance in 3D brain structure reconstruction, achieving a similarity of up

to 85.97% between the original and the generated 3D structure, using only one-fifth of the required amount of images for the traditional stacking method.

As future work, to obtain better pixel resemblance and more details in the generated 2D slices, further improvement can be made with techniques such as combinations of algorithms and assistance from neural networks. In the near future, our method may assist doctors in making more precious diagnoses and better treatments for diseases and injuries, even conquering dementia.

REFERENCES

Aja-Fernández, S. and Vegas-Sánchez-Ferrero, G. (2016). Statistical analysis of noise in mri. *Switzerland: Springer International Publishing*.

AlZu'bi, S., Shehab, M., Al-Ayyoub, M., Jararweh, Y., and Gupta, B. (2020). Parallel implementation for 3d medical volume fuzzy segmentation. *Pattern Recognition Letters*, 130:312–318.

Bail, L. et al. (2009). *The Human Head A Correct Delineation of the Anatomy, Expressions, Features, Proportions and Positions of the Head and Face*. Tom Richardson.

Bathini, P., Brai, E., and Auber, L. A. (2019). Olfactory dysfunction in the pathophysiological continuum of dementia. *Ageing research reviews*, 55:100956.

Bull, D. R. and Zhang, F. (2014). Digital picture formats and representations. *Communicating pictures*, pages 99–132.

Carlson, N. R. and Carlson, N. R. (2007). *Physiology of behavior*. Pearson Boston.

Davis, P. J. (1975). *Interpolation and approximation*. Courier Corporation.

Ebel, K.-D. and Benz-Bohm, G. (1999). *Differential diagnosis in pediatric radiology*. Thieme.

Fajar, A., Sarno, R., Fatichah, C., and Fahmi, A. (2022). Reconstructing and resizing 3d images from dicom files. *Journal of King Saud University-Computer and Information Sciences*, 34(6):3517–3526.

Faragallah, O. S., El-Hoseny, H., El-Shafai, W., Abd El-Rahman, W., El-Sayed, H. S., El-Rabaie, E.-S. M., Abd El-Samie, F. E., and Geweid, G. G. (2020). A comprehensive survey analysis for present solutions of medical image fusion and future directions. *IEEE Access*, 9:11358–11371.

Ghoshal, S., Banu, S., Chakrabarti, A., Sur-Kolay, S., and Pandit, A. (2020). 3d reconstruction of spine image from 2d mri slices along one axis. *IET Image Processing*, 14(12):2746–2755.

Jung, K.-H. and Yoo, K.-Y. (2009). Data hiding method using image interpolation. *Computer Standards & Interfaces*, 31(2):465–470.

Juntu, J., Sijbers, J., Van Dyck, D., and Gielen, J. (2005). Bias field correction for mri images. In *Computer Recognition Systems: Proceedings of the 4th International Conference on Computer Recognition Systems CORES'05*, pages 543–551. Springer.

Lorensen, W. E. and Cline, H. E. (1998). Marching cubes: A high resolution 3d surface construction algorithm. In *Seminal graphics: pioneering efforts that shaped the field*, pages 347–353.

Mustra, M., Delac, K., and Grgic, M. (2008). Overview of the dicom standard. In *2008 50th International Symposium ELMAR*, volume 1, pages 39–44. IEEE.

Nowinski, W. L. (2011). Introduction to brain anatomy. *Biomechanics of the Brain*, pages 5–40.

Patel, A. and Mehta, K. (2012). 3d modeling and rendering of 2d medical image. In *2012 International Conference on Communication Systems and Network Technologies*, pages 149–152. IEEE.

Rajon, D. A. and Bolch, W. E. (2003). Marching cube algorithm: review and trilinear interpolation adaptation for image-based dosimetric models. *Computerized Medical Imaging and Graphics*, 27(5):411–435.

Salerno, J. A., Murphy, D., Horwitz, B., DeCarli, C., Haxby, J. V., Rapoport, S. I., and Schapiro, M. B. (1992). Brain atrophy in hypertension. a volumetric magnetic resonance imaging study. *Hypertension*, 20(3):340–348.

Senthilkumaran, N. and Thimmiaraja, J. (2014). Histogram equalization for image enhancement using mri brain images. In *2014 World congress on computing and communication technologies*, pages 80–83. IEEE.

Statistics Bureau (2023). Population and households. In *JAPAN STATISTICAL YEARBOOK 2024*, chapter 2, pages 29–82. Ministry of Internal Affairs and Communications, Tokyo.

Thanh, C. Q. and Hai, N. T. (2017). Trilinear interpolation algorithm for reconstruction of 3d mri brain image. *American Journal of Signal Processing*, 7(1):1–11.

van der Flier, W. M. and Scheltens, P. (2005). Epidemiology and risk factors of dementia. *Journal of Neurology, Neurosurgery & Psychiatry*, 76(suppl 5):v2–v7.

Wang, Z., Bovik, A. C., Sheikh, H. R., and Simoncelli, E. P. (2004). Image quality assessment: from error visibility to structural similarity. *IEEE transactions on image processing*, 13(4):600–612.